

# RSC Advances



This is an *Accepted Manuscript*, which has been through the Royal Society of Chemistry peer review process and has been accepted for publication.

*Accepted Manuscripts* are published online shortly after acceptance, before technical editing, formatting and proof reading. Using this free service, authors can make their results available to the community, in citable form, before we publish the edited article. This *Accepted Manuscript* will be replaced by the edited, formatted and paginated article as soon as this is available.

You can find more information about *Accepted Manuscripts* in the [Information for Authors](#).

Please note that technical editing may introduce minor changes to the text and/or graphics, which may alter content. The journal's standard [Terms & Conditions](#) and the [Ethical guidelines](#) still apply. In no event shall the Royal Society of Chemistry be held responsible for any errors or omissions in this *Accepted Manuscript* or any consequences arising from the use of any information it contains.



## Fabrication and application of non-rare earth red phosphors for warm white-light-emitting diodes

Qiang Zhou,<sup>a</sup> Yayun Zhou,<sup>a</sup> Zhengliang Wang,<sup>\*a</sup> Yong Liu,<sup>a</sup> Guo Chen,<sup>a</sup> Jinhui Peng,<sup>a</sup> Jing Yan<sup>b</sup> and Mingmei Wu<sup>\*b</sup>

Received 00th August 2015,  
Accepted 00th August 2015

DOI: 10.1039/x0xx00000x

www.rsc.org/

In this work, a facile and efficient method for the preparation of  $K_2XF_6:Mn^{4+}$  ( $X = Si, Ti$  and  $Ge$ ) red phosphor is reported. They were synthesized by adding KF to precipitate the warm mixed solution with  $XO_2$ ,  $KMnO_4$  and HF as raw materials. After the doping of  $Mn^{4+}$ , though the obtained products exhibit irregular micro-sized particulate morphologies, they present the same single phases as their matrixes and no impurity can be examined. The optical properties of the fluoride complexes were investigated by photo-luminescent spectra, diffuse reflectance spectrum, and luminescence decay curves. They presented bright red emission under blue light illumination, and the warm white-light-emitting diodes with low correlated color temperature, high color rendering index and high luminous efficiency, such as 3156 K, 84.9 and 138.4  $lm \cdot W^{-1}$ , were achieved by coating the mixture of red phosphor with commercial  $Y_3Al_5O_{12}:Ce^{3+}$  on blue-GaN chips.

### Introduction

After the creative invention of efficient blue light-emitting diodes (LEDs), bright white light source, typically white-light-emitting diode (WLED), has been enabled and received a great deal of interest to scientists and engineers due to their long lifetime, energy-saving and environment-friendly properties.<sup>1-3</sup> To obtain high luminous efficient white light, nowadays, the WLEDs are always fabricated from the merger of yellow  $Y_3Al_5O_{12}:Ce^{3+}$  (denoted as YAG) phosphor with blue LED chips.<sup>4,5</sup> However, the WLEDs fabricated by such approach lack red emission in the luminescence spectra,<sup>6,7</sup> this restricts their application in indoor lighting due to the high correlated color temperature (CCT > 4,000 K) and low color rendering index (CRI,  $R_o < 80$ ).<sup>8-11</sup> To solve this problem, enormous research efforts have been devoted to explore red phosphors with great luminous efficiency. For example, rare-earth-activated sulfides and nitrides have been reported to fabricate warm WLEDs.<sup>12,13</sup> Though these materials exhibit fascinating luminescence, the unstable chemical property and harsh

preparation process limit their application in WLEDs, needless to say their broadband emission beyond 650 nm decreases the luminous efficiency and the sensitivity of human eyes.<sup>14</sup>

Recently,  $Mn^{4+}$  activated red fluoride phosphors have been attracted a number of research interest since its  $d-d$  transition in symmetry octahedral crystal field, which causes the broadband adsorption in blue region and narrowband emission in red range respectively.<sup>15,16</sup> As it known to all,  $Mn^{4+}$  is sensitive to surrounding environment and hard to be controlled. Hence, different synthesis routes have been developed to prepare  $Mn^{4+}$  doped fluoride complexes. The group of Adachi reported a series of red fluoride phosphors,  $K_2XF_6:Mn^{4+}$  ( $X = Sn, Ge$  or  $Si$ ), through a wet chemical etching route in aqueous  $KMnO_4$  and HF mixed solution.<sup>17-19</sup> For example, a cation exchange method was proposed by the group of Chen to prepare  $K_2TiF_6:Mn^{4+}$  and  $K_2SiF_6:Mn^{4+}$  red phosphors by mixing fluoride hosts with  $K_2MnF_6$  powders in HF solution.<sup>14</sup> A co-precipitation method for the preparation of  $Na_2SiF_6:Mn^{4+}$ ,  $K_2SiF_6:Mn^{4+}$  and  $K_2GeF_6:Mn^{4+}$  red phosphors was established by Liu and his co-authors with the use of  $H_2O_2$  as reductant to reduce  $Mn^{7+}$  to  $Mn^{4+}$ .<sup>20-22</sup> Pan and her colleagues demonstrated a hydrothermal method for the synthesis of  $Mn^{4+}$  doped fluorides, such as  $K_2SiF_6:Mn^{4+}$ ,  $BaSiF_6:Mn^{4+}$ ,  $BaTiF_6:Mn^{4+}$  and  $K_2TiF_6:Mn^{4+}$  phosphors.<sup>23-26</sup> As well, in our previous work,  $BaGeF_6:Mn^{4+}$  and  $Cs_2TiF_6:Mn^{4+}$  red phosphors were synthesized and their potential applications in WLED devices were investigated.<sup>4,27</sup> Despite the successes, all of the approaches have some drawbacks. Specifically, the product yield of etching technique is very low, the starting materials of co-precipitation and cation exchange routes are either expensive or complicated to be prepared, and the reaction temperature of hydrothermal method is very high, leading to low doping concentration of  $Mn^{4+}$ . In a word, up to now, the red

<sup>a</sup> Key Laboratory of Comprehensive Utilization of Mineral Resource in Ethnic Regions, Joint Research Centre for International Cross-border Ethnic Regions Biomass Clean Utilization in Yunnan, School of Chemistry & Environment, Yunnan Minzu University, Kunming, 650500, P. R. China.

<sup>b</sup> MOE Key Laboratory of Bioinorganic and Synthetic Chemistry, School of Chemistry and Chemical Engineering, Sun Yat-Sen (Zhongshan) University, Guangzhou, 510275, P. R. China.

Email: wangzhengliang@foxmail.com, ceswmm@mail.sysu.edu.cn.

<sup>†</sup> Electronic Supplementary Information (ESI) available: Details to the relationship between reaction time and PL properties of the obtained  $K_2GeF_6:Mn^{4+}$  and  $K_2SiF_6:Mn^{4+}$  red phosphors, as well the AAS results of  $K_2TiF_6:Mn^{4+}$  and the WLED performance and corresponding CIE chromaticity diagram data. See DOI: 10.1039/x0xx00000x

fluoride phosphor could not be produced efficiently and the doping amount of  $Mn^{4+}$  is hard to control. Therefore, from a practical point of view, it appears very urgent and important to develop a facile and efficient way to maturely control the formation and occupation of  $Mn^{4+}$  while using simple raw materials.

In this paper, we will present a facile and efficient one-step precipitation method to prepare single-phase  $K_2XF_6:Mn^{4+}$  ( $X = Si, Ti$  or  $Ge$ , denoted as  $KXFM$ ) red phosphors only employing simple and commercial starting materials. The doping amount of  $Mn^{4+}$  can be controlled by reaction time with excessive amount of  $KMnO_4$ . The effect of reaction time on the photo-luminescent properties of the  $KXFM$  red phosphor has been determined. All the obtained products emit intensive red emission under blue light illumination, implying the  $Mn^{4+}$  doped fluoride phosphors are potential red components for warm WLEDs.

## Experimental

**Materials.** All source materials in this work, including hydrofluoric acid, potassium permanganate, potassium fluoride, silicon oxide, titanium oxide and germanium oxide were of analytical grade and without any purification prior to use. The commercial YAG yellow phosphor was purchased from Shenzhen Quanjing Photon Co. Ltd., China.

**Synthesis.** Red fluoride phosphors were synthesized *via* a facile one-step precipitation method with a mild heating process. In a typical synthesis, 5 mmol  $TiO_2$  (or  $SiO_2, GeO_2$ ) was put into a plastic beaker containing 10 ml magnetically stirring 40% HF solution until completely dissolved. Thereafter, 2 mmol  $KMnO_4$  and 16 mmol  $KF$  were added into the colorless transparent solution in order, which was subsequently kept at  $50^\circ C$  only for 15 min. Then  $K_2TiF_6:Mn^{4+}$  (KTFM) precipitation was found at the bottom of the plastic beaker. Finally, the resulting solid product was collected carefully from the plastic beaker, washed extensively with distilled water and methanol for several times respectively, and dried at  $80^\circ C$  for 2 hours. The schematic diagram of this precipitation process is shown in Figure 1.

The WLEDs were fabricated by coating YAG yellow phosphor with or without  $K_2XF_6:Mn^{4+}$  ( $X = Si, Ti$  and  $Ge$ ) (denoted as  $KXFM$ ) on GaN chips. These LEDs were operated at 5.0 V reverse voltage with a forward current of 20 mA.

**Characterizations.** The crystal structure of the as-prepared samples was investigated on a powder X-ray diffraction (XRD) with an X-ray diffractometer using  $Cu K\alpha$  radiation ( $\lambda = 0.15406$  nm) and a graphite monochromator. The corresponding surface morphology and microstructure were observed on a scanning electron microscopy (SEM, FEI Quanta 200 Thermal FE Environment scanning electron microscopy) with an attached energy-dispersive X-ray spectrometer (EDS). Compositional analysis was performed on a Shimadzu AA-6300 atomic absorption spectrophotometer (AAS). The Diffuse Reflectance Ultraviolet-Visible spectra (DRS) and decay curve were collected on a Cary 5000 UV-Vis-NIR spectrophotometer and an Edinburgh FLS920 combined fluorescence lifetime and steady state spectrometer, respectively. The photo-luminescent properties were measured on a Cary Eclipse FL1011M003 (Varian) spectrofluorometer with xenon lamp as excitation light source. The

performance of WLEDs was recorded on a high accurate array spectrometer (HSP6000).

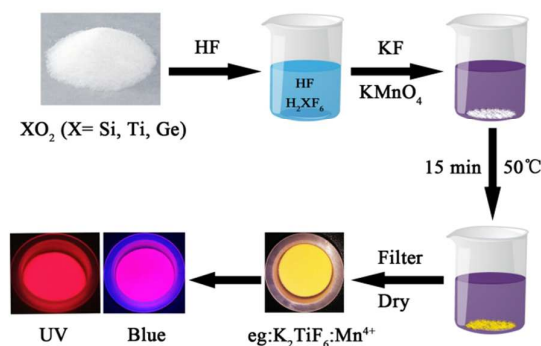


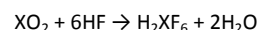
Fig. 1 Schematic illustration of the preparation process.

## Results and discussion

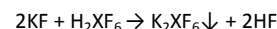
### Mechanism, Composition and Morphology Analysis.

Previously,  $H_2O_2$  was employed as reductant to promote the reduction process of  $Mn^{7+}$  to  $Mn^{4+}$  for the preparation of  $Na_2SiF_6:Mn^{4+}$  red phosphor since the slow redox rate between  $KMnO_4$  and HF at ambient temperature.<sup>20</sup> In this work, a mild heat treatment at  $50^\circ C$ , together with an excessive amount of  $KMnO_4$  were adopted to accelerate the formation of  $Mn^{4+}$ , which was simultaneously coordinated with surrounding  $F^-$  to form stable  $MnF_6^{2-}$  octahedron. Generally, because of the existence of excessive amount of  $KMnO_4$ , the upper solution kept a purple color during the preparation process.

According to the experimental phenomena of the preparation process, we presumed that the chemical stability of our  $KXFM$  products toward hydrolysis is better than the rare-earth doped sulphides since a series of reactions occurred. Firstly, the  $XO_2$  precursor was dissolved into colorless transparent solution in 40 % HF concentration and no precipitation could be found at the bottom of the reaction beaker. The reaction formula is as follows:



Because of the low solubility of  $K_2XF_6$  in HF solution, when  $KF$  was put into the purple solution,  $K^+$  could substitute  $H^+$  to form  $K_2XF_6$ , which was precipitated from the clear solution. This precipitation reaction can be clearly observed.



After the addition of  $KMnO_4$ ,  $Mn^{7+}$  can be transformed into  $Mn^{4+}$  in concentrated HF environment. Mild heat treatment could accelerate the redox rate of this transformation process, which could be expressed as:



As we know, the ionic radius and coordination number of  $Mn^{4+}$  ( $0.53 \text{ \AA}$ ,  $CN = 6$ ) in concentrated HF solution are similar as  $Si^{4+}$  ( $0.40 \text{ \AA}$ ,  $CN = 6$ ),  $Ti^{4+}$  ( $0.60 \text{ \AA}$ ,  $CN = 6$ ) and  $Ge^{4+}$  ( $0.53 \text{ \AA}$ ,  $CN = 6$ ), which is beneficial for the substitution of  $Mn^{4+}$  for  $X^{4+}$  in  $XF_6^{2-}$  group since

cation exchange between them. This is why KXF<sub>6</sub> red phosphor can be easily produced from the clear solution using this one-step precipitation method.

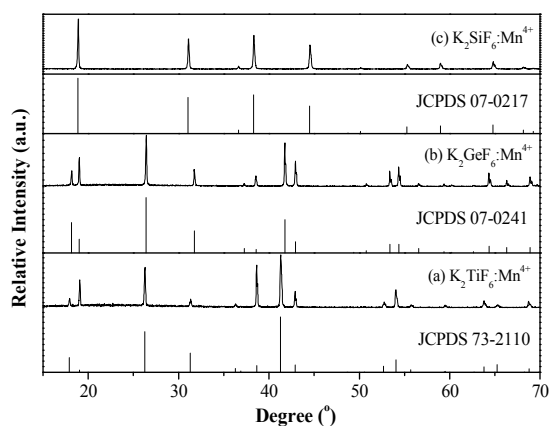


**Fig. 2** Representative XRD patterns of the obtained (a) KTFM, (b) KGFM and (c) KSFM products.

Figure 2 exhibits the X-ray diffraction (XRD) patterns of the obtained  $K_2TiF_6:Mn^{4+}$  (KTFM),  $K_2GeF_6:Mn^{4+}$  (KGFM) and  $K_2SiF_6:Mn^{4+}$  (KSFM) products, along with their corresponding standard diffraction cards. In curve either a or b, all the diffraction peaks can be indexed to the space group  $P-3m1$  of either hexagonal  $K_2TiF_6$  (JCPDS No. 73-2110,  $a = b = 5.715 \text{ \AA}$  and  $c = 4.656 \text{ \AA}$ ) or  $K_2GeF_6$  (JCPDS No. 07-0241,  $a = b = 5.632 \text{ \AA}$  and  $c = 4.668 \text{ \AA}$ ), no secondary impurity can be identified, indicating that either KTFM or KGFM product has single phase, and the introduction of  $Mn^{4+}$  does not change the crystal structure of either  $K_2TiF_6$  or  $K_2GeF_6$  matrix. As illustrated above, that is because  $Mn^{4+}$  not only has the identical valence state, but also the similar ionic radius as either  $Ti^{4+}$  or  $Ge^{4+}$ , which results in the replacement of  $Mn^{4+}$  for the lattice site of either  $Ti^{4+}$  or  $Ge^{4+}$  easily. Both the crystal structures of  $K_2TiF_6$  and  $K_2GeF_6$  are displayed in Figure 3a and b (insert images). Each  $Ti^{4+}$  (or  $Ge^{4+}$ ) coordinated with 6  $F^-$  to form a regular  $TiF_6^{2-}$  (or  $GeF_6^{2-}$ ) octahedron, and  $K^+$  is at the center of 12 neighboring  $F^-$ . When the occupation of  $Mn^{4+}$  occurred,  $Mn^{4+}$  occupies the octahedral core site of  $Ti^{4+}$  (or  $Ge^{4+}$ ) to coordinate with 6  $F^-$  anions forming stable  $MnF_6^{2-}$  octahedron. Similar results can be obtained from curve c of KSFM (JCPDS No. 07-0217,  $a = b = c = 8.133 \text{ \AA}$ ) in Figure 2 except its crystal structure (inset of Figure 3c). It belongs to cubic  $Fm\bar{3}m$  space group.  $Si^{4+}$  takes up the vertex and face-centered position of the cubic unit cell, and 4  $K^+$  ions are uniformly distributed inside the cube. Each  $Si^{4+}$  is surrounded by 6  $F^-$  to form a regular  $SiF_6^{2-}$  octahedron.

The representative morphology and composition results of the afore-discussed three products are displayed in Figure 3. Obviously, the SEM image of Figure 3a1 illustrates that the obtained KTFM product is composed of a number of irregular micro-sized particulate crystals, ranging from 5 to 50  $\mu m$ , with clear edges and corners. This indicates the KTFM product was in good crystallization. The corresponding EDS spectrum exhibited the existence of F, Ti, K,

and Mn elements and the absence of O one, suggesting that Mn element has been well doped into the  $K_2TiF_6$  matrix and no  $MnO_2$  is produced during the entire precipitation process. This result confirmed that this precipitation method is a facile and beneficial route for the substitution of  $Mn^{4+}$  for  $Ti^{4+}$  in matrix lattice. Moreover, the morphology results of two other products, KGFM and KSFM in Figure 3b-c, are also composed of a series of micro-sized particles, distributing from 10 to 30  $\mu m$  (Figure 3b) and from 5 to 10  $\mu m$  (Figure 3c) with clear particulate edges and corners.

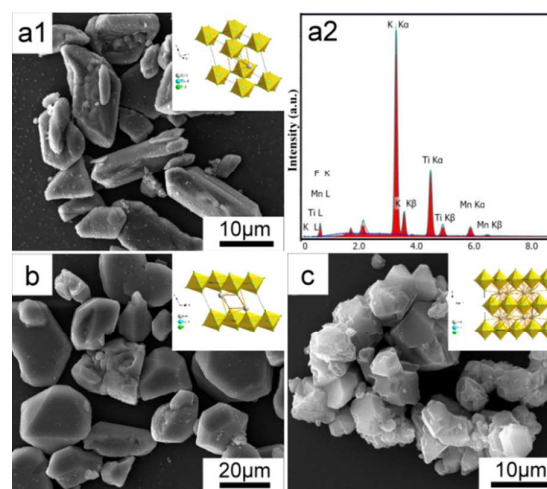


**Fig. 3** The SEM images, crystal structures and representative EDS spectrum of the as-synthesized (a) KTFM, (b) KGFM and (c) KSFM products.

#### Optical properties and Application in WLEDs

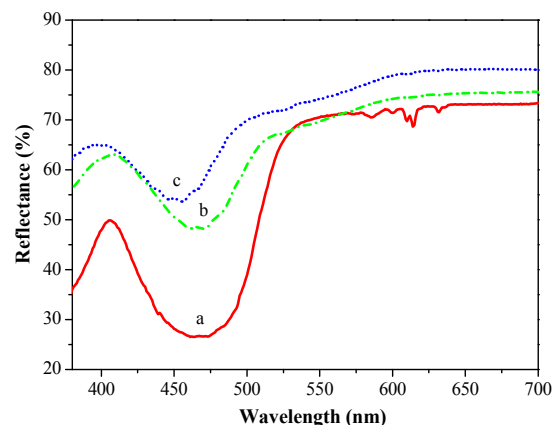


**Fig. 4** DRS spectra of the as-synthesized (a) KTFM, (b) KGFM and (c) KSFM products.

The diffuse reflectance spectra (DRS) of the obtained KTFM, KGFM and KSFM products were shown in Figure 4. Evidently, all of them revealed a similar broad adsorption band around 460 nm in the blue region, with the strongest peak locating at 463, 460 and 455 nm respectively. This is similar to the adsorption property of  $Mn^{4+}$  ion-activated red fluoride phosphor, most likely originates from the spin-allowed transition of  $Mn^{4+}$  from ground state  $^4A_2$  to excited

state  ${}^4T_2$ . Furthermore, the strongest adsorption peak position from curve a to c apparently blue shifted, which can be attributable to their different crystal field strengths. For comparison,  $TiF_6^{2-}$  possesses weaker crystal field strength than that of  $GeF_6^{2-}$  and  $SiF_6^{2-}$  because the bigger ionic radius of  $Ti^{4+}$  than  $Ge^{4+}$  and  $Si^{4+}$ . In a word,  $TiF_6^{2-}$  possess the weakest crystal field strength among them, which leads to the blue shift behavior from curve a to c in Figure 4. Actually, according to the Inorganic Crystal Structure Database (ICSD) results, bond distances of Ti-F, Ge-F and Si-F are 1.9171, 1.7703 and 1.6829 Å (ICSD No. 24659, 24026 and 79407) respectively, which results in  $TiF_6^{2-}$  possesses weaker crystal field strength and hence longer excitation wavelength than those of the  $GeF_6^{2-}$  and  $SiF_6^{2-}$ . Furthermore, in Figure 4, it can be clearly observed that the KTFM phosphor exhibits obviously stronger adsorption ability than those of two others, which may lead to its better emission property.

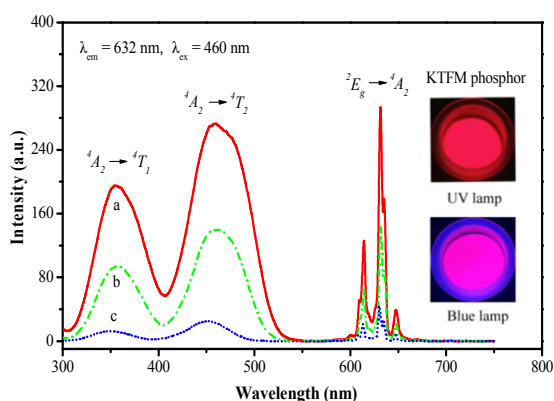


**Fig. 5** PLE and PL spectra of (a) KTFM, (b) KGFM and (c) KSFM products with representative photographs of KTFM phosphor illuminated under UV and blue lamp respectively.

In order to prove the above DRS results, the photoluminescence excitation (PLE) and photoluminescence (PL) spectra of the obtained KXFM products were investigated and shown in Figure 5. It is clear that except the same broad adsorption band as DRS result, the three excitation spectra still exhibit a broad adsorption band in the UV region, which is due to the spin-allowed transition of  $Mn^{4+}$  from ground state  ${}^4A_{2g}$  to excited state  ${}^4T_{1g}$ . The full width at half maximum (FWHM) for KTFM, KGFM and KSFM at 460 nm are about 65, 60 and 50 nm respectively, much broader than that of blue GaN chip emission ( $\sim 20$  nm). This demonstrates three KXFM phosphors can effectively absorb the emitted blue light from GaN chip. The three main sharp peaks lines from 600 to 650 nm strongly indicated that the emission light of these phosphors is red, which are ascribed to the spin-forbidden  $d-d$  transition of  $Mn^{4+}$  between  ${}^2E_g$  and  ${}^4A_{2g}$ . Obviously, the red emission in the PL spectra was a typical property of  $Mn^{4+}$  ion-activated phosphors as reported previously.<sup>28,29</sup> This strongly indicates that the  $Mn^{4+}$  ions have been doped into the  $K_2XF_6$  matrixes. Moreover, the red light emitted from KTFM phosphor presents stronger intensity than those of two other products, which was coincidence with the DRS assumption demonstrated above.

The influence of reaction time on the PL properties of the as-prepared KTFM red phosphors was shown in Figure 6. It exhibits the emission spectra of KTFM phosphors prepared with  $0.2 \text{ mol}\cdot\text{L}^{-1}$   $KMnO_4$  for 5, 10, 15, 20, 30, 60, 75 and 90 min under 460 nm blue light excitation. Evidently, these spectral shapes are similar and each of them is composed of three main sharp lines distributed in the range of 610–650 nm with the strongest peak at 631 nm. This red emission originates from the aforementioned spin-forbidden  $d-d$  transition from  ${}^2E_g$  to  ${}^4A_{2g}$  of  $Mn^{4+}$ .<sup>20–22</sup> The influence of reaction time on the emission intensity of KTFM is very clear. Only reacted for 15 min, the obtained KTFM phosphor could emit the strongest red light, which further verifies this synthesis route is efficient in fabricating  $Mn^{4+}$  doped red phosphor. Furthermore, no emission peak position shifts when the reaction time changes. This is because the  ${}^2E_g$  energy state in the  $d^3$  electronic configuration is independent of crystal field, which results in the emission transition position of  ${}^2E_g \rightarrow {}^4A_{2g}$  is independent on its crystal field strength. Gradually prolonging the reaction time from 15 to 90 min, the emission dropped, which definitely resulted from the concentration quenching of  $Mn^{4+}$  in  $K_2TiF_6$  crystal lattice.

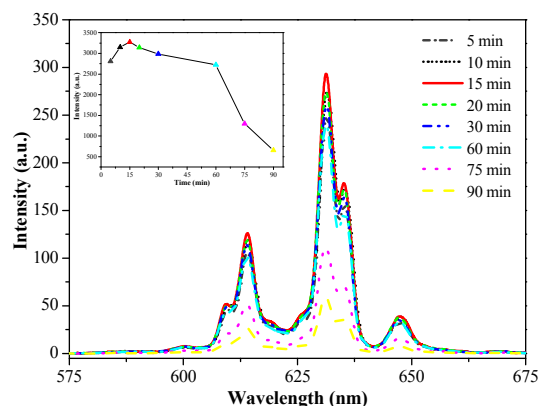


**Fig. 6** The PL spectra of KTFM red phosphors obtained from 40% HF with different reaction time, and recorded at room temperature. Insert is the dependence of PL intensity on reaction time.

In order to further confirm the concentration quenching phenomenon and determine the quenching concentration of  $Mn^{4+}$  in  $K_2TiF_6$  crystal lattice, a 68 % concentrated  $HNO_3$  solution was employed to dissolve KTFM powders and atomic absorption spectrophotometer (AAS) aforementioned in characterizations was adopted to measure the relative concentration of  $Mn^{4+}$ . Results were presented in Table S1. Obviously, with the extension of reaction time, the substitution amount of  $Mn^{4+}$  for  $Ti^{4+}$  in  $K_2TiF_6$  host indeed exhibits a rising tendency. According to the PL results obtained above, the product reacted for 15 min presents the strongest PL intensity, which means that the optimum doping concentration of  $Mn^{4+}$  in our work is 4.9 %. Once more  $Mn^{4+}$  ions were doped into  $K_2TiF_6$  matrix, the PL intensity dropped contrarily, which indicated that the PL property of KTFM red phosphor is highly dependent on the doping amount of  $Mn^{4+}$ . Through controlling the reaction time, its PL property can be rationally tuned. The production efficiency of  $K_2TiF_6:Mn^{4+}$  in this work as short as 15 min

at 50 °C, is extremely great. The quenching phenomenon also occurred in KGFM and KSFM phosphors (Figure S1 in ESI†), and their optimum reaction times are 60 and 30 min respectively. The dependence of PL intensity and doping amount of KTFM phosphor on reaction time was shown in the inset of Figure 6.

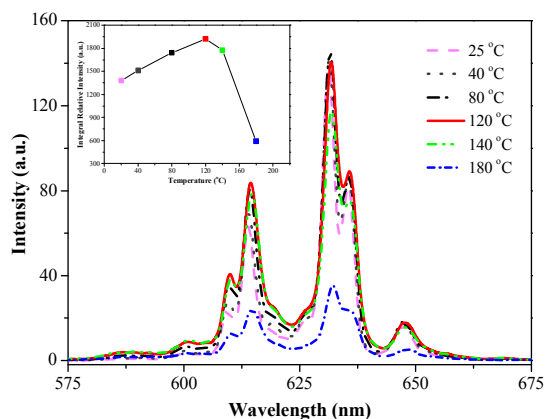


**Fig. 7** Temperature-dependent thermal luminescent spectra of KTFM red phosphor and the relationship between integral relative intensity and temperature.

The influence of temperature on the PL properties of KTFM red phosphor is shown in Fig. 7. It can be clearly observed that, with the temperature increasing, the emission peak position does not shift. Up to 120 °C, nearly 139% of the integral emission intensity can be preserved compared with that at 25 °C, which demonstrate its excellent thermal luminescent property at high temperatures. The thermal luminescent property of KGFM and KSFM are nearly the same as KTFM phosphor (Figure S2 in ESI†). Their PL decay properties of the prepared KTFM, KGFM and KSFM red phosphors were operated at room temperature (Figure S3 in ESI†). Apparently, three PL decay curves are well fitted into single-exponential function. Based on this characteristic, their PL lifetimes were determined as 4.7, 5.8 and 7.1 ms respectively. This result complements the experimental data of previous reports prepared by other methods.

The WLED performance of YAG and YAG-KTFM mixture was evaluated and the difference was shown in Figure 8. Only with the existence of YAG powders, cold bright white light was observed by naked eyes, whose electroluminescence spectrum still displays an intensive emission of GaN (~ 450 nm), indicating this kind of WLED is an appropriate acceptor for the combination of KTFM red phosphor. After the addition of KTFM products, sharp red emission lines of  $Mn^{4+}$  in the EL spectrum and bright red light can be observed (Figure 8b), which means the addition of KTFM is favorable for the improvement of CRI and CCT levels of the YAG type WLED. Without the use of KTFM, the CRI and CCT are 72.8 and 6315 K respectively, while with the addition of KTFM, these data gradually change to be 84.9 and 3156 K, with an extraordinary luminous efficiency of  $138.4 \text{ lm}\cdot\text{W}^{-1}$  (Figure S4 and Table S2 in ESI†). The white light emitted from the YAG-KTFM system is much warmer. According the survey of reference 14, warm WLEDs based on KTFM red phosphor presents a luminous efficacy of  $124 \text{ lm}\cdot\text{W}^{-1}$

under 20 mA drive current.<sup>14</sup> In this work, with the same drive current, the fabricated KTFM type WLED shows a higher luminous efficacy of  $138.4 \text{ lm}\cdot\text{W}^{-1}$ . This indicates the KTFM red phosphor is a promising candidate for extending the current commercial WLEDs application although its precipitation route is facile and efficient. The performance of other WLEDs is summarized in Figure S5 and Table S2 in ESI†.

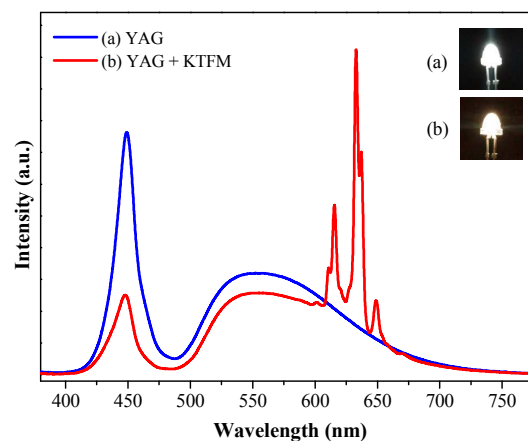


**Fig. 8** Electroluminescence spectra and corresponding bright white light images of the WLEDs fabricated (a) without and (b) with  $K_2TiF_6:Mn^{4+}$  red phosphor evaluated with 20 mA forward current.

## Conclusions

In this work, we have reported a facile and efficient precipitation route with very simple starting materials to fabricate phase-pure fluoride  $K_2XF_6:Mn^{4+}$  ( $X = Si, Ti$  and  $Ge$ ) red phosphors without any impurities. The as-prepared products can absorb broadband blue light and emit intense bright narrowband red light. Their PL intensity can reach the highest even if a short reaction period has been employed. With the use of these  $Mn^{4+}$  doped fluoride red phosphors in WLED devices, obvious improvement in CRI and CCT data ( $R_o = 84.9$  and  $CCT = 3156 \text{ K}$ ) has been achieved, whilst keeping an extraordinary luminous efficiency of  $138.4 \text{ lm}\cdot\text{W}^{-1}$ . Simple preparation process and efficient red luminescence under blue light excitation make this precipitation approach be an efficient and general way to prepare  $K_2XF_6:Mn^{4+}$  as promising phosphors.

## Acknowledgements

This work was financially supported by the National Natural Science Foundation of China, the Natural Science Foundation of Yunnan Province (Grants 21261027 and 2014FB147), the Joint Funds of the National Natural Science Foundation of China and Guangdong Province, Research Fund for the Doctoral Program of Higher Education of China, and Guangdong Province for industrial applications of rare earth materials (Grants U1301242, 20130171130001, and 2012B09000026).

## References

- 1 W. T. Chen, H. S. Shen, R. S. Liu, J. P. Attfield, *J. Am. Chem. Soc.*, 2012, **134**, 8022.
- 2 I. Ahemen, K. DeDilip and A. N. Amah, *Appl. Phys. Res.*, 2014, **6**, 95.
- 3 M. H. Chang, D. Das, P. V. Varde and M. Pecht, *Microelectron. Reliab.*, 2012, **52**, 762.
- 4 Q. Zhou, Y. Y. Zhou, Y. Liu, L. J. Luo, Z. L. Wang, J. H. Peng, J. Yan, and M. M. Wu, *J. Mater. Chem. C*, 2015, **3**, 3055.
- 5 C. C. Lin, and R. S. Liu, *J. Phys. Chem. Lett.*, 2011, **2**, 1268.
- 6 P. Pust, V. Weiler, C. Hecht, A. Tucks, A. S. Wochnik, A. K. Hen, D. Wiechert, C. Scheu, P. J. Schmidt and W. Schnick, *Nat. Mater.*, 2014, **13**, 891.
- 7 P. H. Chuang, C. C. Lin, H. Yang and R. S. Liu, *J. Chin. Chem. Soc.*, 2013, **60**, 801.
- 8 P. Schlotter, R. Schmidt and J. Schneider, *Appl. Phys. A*, 1997, **64**, 417.
- 9 T. S. Chan, R. S. Liu and I. Baginskiy, *Chem. Mater.*, 2008, **20**, 1215.
- 10 R. Zhang, H. Lin, Y. L. Yu, D. Q. Chen, J. Xu and Y. S. Wang, *Laser Photonics Rev.*, 2014, **8**, 158.
- 11 G. G. Li, D. L. Geng, M. M. Shang, C. Peng, Z. Y. Cheng and J. Lin, *J. Mater. Chem.*, 2011, **21**, 13334.
- 12 C. F. Guo, D. X. Huang, Q. Su, *Mater. Sci. Eng. B*, 2006, **130**, 189.
- 13 X. X. Duan, S. H. Huang, F. T. You, K. Kang, *J. Rare Earth*, 2009, **27**, 43.
- 14 H. M. Zhu, C. C. Lin, W. Q. Luo, S. T. Shu, Z. G. Liu, Y. S. Liu, J. T. Kong, E. Ma, Y. G. Cao, R. S. Liu, X. Y. Chen, *Nat. Commun.*, 2014, **5**, 4312:1.
- 15 Y. K. Xu and S. Adachi, *J. Appl. Phys.*, 2009, **105**, 013525.
- 16 C. X. Liao, R. P. Cao, Z. J. Ma, Y. Li, G. P. Dong, K. N. Sharafudeen and J. R. Qiu, *J. Am. Ceram. Soc.*, 2013, **96**, 3552.
- 17 Y. Arai, T. Takahashi and S. Adachi, *Opt. Mater.*, 2010, **32**, 1095.
- 18 S. Adachi and T. Takahashi, *J. Appl. Phys.*, 2009, **106**, 013516.
- 19 S. Adachi and T. Takahashi, *J. Appl. Phys.*, 2008, **104**, 023512.
- 20 H. D. Nguyen, C. C. Lin, M. H. Fang and R. S. Liu, *J. Mater. Chem. C*, 2014, **2**, 10268.
- 21 L. L. Wei, C. C. Lin, M. H. Fang, M. G. Brik, S. F. Hu, H. Jiao and R. S. Liu, *J. Mater. Chem. C*, 2015, **3**, 1655.
- 22 L. L. Wei, C. C. Lin, Y. Y. Wang, M. H. Fang, H. Jiao and R. S. Liu, *ACS Appl. Mater. Interfaces*, 2015, **7**, 10656.
- 23 L. F. Lv, X. Y. Jiang, S. M. Huang, X. A. Chen and Y. X. Pan, *J. Mater. Chem. C*, 2014, **2**, 3879.
- 24 X. Y. Jiang, Y. X. Pan, S. M. Huang, X. A. Chen, J. G. Wang, G. K. Liu, *J. Mater. Chem. C*, 2014, **2**, 2301.
- 25 X. Y. Jiang, Z. Chen, S. M. Huang, J. G. Wang and Y. X. Pan, *Dalton Trans.*, 2014, **43**, 9414.
- 26 L. L. Lv, Z. Chen, G. K. Liu, S. M. Huang and Y. X. Pan, *J. Mater. Chem. C*, 2015, **3**, 1935.
- 27 Q. Zhou, Y. Y. Zhou, Y. Liu, Z. L. Wang, G. Chen, J. H. Peng, J. Yan and M. M. Wu, *J. Mater. Chem. C*, 2015, **3**, 9615.
- 28 J. H. Oh, H. Kang, Y. J. Eo, H. K. Park and Y. R. Do, *J. Mater. Chem. C*, 2015, **3**, 607.
- 29 T. N. Ye, S. Li, X. Y. Wu, M. Xu, X. Wei, K. X. Wang, H. L. Bao, J. Q. Wang and J. S. Chen, *J. Mater. Chem. C*, 2013, **1**, 4327.

### Graphical Abstract

A facile and efficient solution chemistry route with very simple starting materials has been proposed for the synthesis of phase-pure  $\text{K}_2\text{XF}_6:\text{Mn}^{4+}$  (X = Si, Ti and Ge) red phosphors, which can absorb broadband blue light and emit intense bright narrowband red light, and can be used in white-light-emitting diodes to efficiently improve their performance for their applications in indoor lighting.

